Wind and Structures, Vol. 16, No. 2 (2013) 213-224
DOI: http://dx.doi.org/10.12989/was.2013.16.2.213

Guide plates on wind uplift of a solar collector model

K.M. Chung *1 , K.C. Chang[2] , C.K. Chen[2] and C.C. Chou[2]

[1]*Aerospace Science and Technology Research Center, National Cheng Kung University, Tainan, Taiwan*
[2]*Department of Aeronautics and Astronautics, National Cheng Kung University, Tainan, Taiwan*

(Received May 14, 2010, Revised April 22, 2011, Accepted February 1, 2012)

Abstract. One of the key issues affecting the promotion of solar water heaters in Taiwan is the severe impact of typhoon each year. An experimental study was conducted to investigate the wind uplift characteristic of a solar collector model with and without a guide plate. The guide plate with different lengths and orientations with respect to wind direction was adopted. It is found that the wind uplift of a solar collector is associated with the tilt angle of the flat panel as expected. A cavity formed between the guide plate and the flat panel has a significant effect on the distributions of streamwsie and lateral pressure. Reduction in uplift is essentially coupled with the projected area of a guide plate on the lower surface of the tilt flat panel.

Keywords: guide plate; solar collector; uplift; wind load, typhoon

1. Introduction

Under the incentive programs of the government, solar water heaters (SWHs) in Taiwan have been promoted within the last two decades (Chang *et al*. 2006, 2008, 2009). A growing number of SWHs have been installed on the flat roof of buildings each year. Furthermore, most previous studies on SWHs have focused on the thermal efficiency of various types of solar collectors (Kalogirou 2004). Only limited works have been done on the aerodynamic characteristics of solar collectors and their supporting structure (Kopp *et al*. 2002, Radu *et al*. 1986, Wood *et al*. 2001). However, typhoons are among the natural hazards that incur costly impact on residential construction (Oaulotto *et al*. 2006, Li *et al*. 2008, Li *et al*. 2009). In summer, tens of typhoons may occur over the western North Pacific and South China Sea each year, and some affect Taiwan (Lee 2009, Chang *et al*. 2010). The safety of SWHs under severe wind load during typhoon season should be addressed. In particular, glasses of solar collectors are broken mainly due to strong wind uplift and its resultant large deflection. Therefore, a good estimation of resistance to wind uplift and reduction in aerodynamic loads of solar collectors is prerequisite to prevent such damage. A previous experimental study was conducted by Chung *et al*. (2008) to investigate the wind uplift of lifted solar collector models with and without a guide plate. At a tilt angle of 25^o, the localized load of a solar collector is significant near the front edge. Reduction of wind uplift with is observed with a guide plate and effects of the incremental height of a solar collector are less significant. Note that Reynolds number independence is also observed. Furthermore, Taiwan is

*Corresponding author, Research Fellow, E-mail: kmchung@mail.ncku.edu.tw

situated between 22°N and 25°N and the tilt angle of most solar collectors ranges from 15° to 30°. The optimum geometry of a guide plate on uplift reduction of a solar collector model should also be addressed. In the present study, the effects of tilt angle of a solar collector and the geometry of a guide plate are investigated. A thin film of the mixture (titanium dioxide, oil, oleic acid and kerosene) is also applied on the upper and lower surface of the tilted flat panel to visualize the surface flow pattern.

2. Experimental setup

The experiments were conducted in the low-speed wind tunnel at the Aerospace Science and Technology Research Center, National Cheng Kung University (ASTRC/ NCKU). The tunnel is a closed-loop type. The facility consists of a 450 HP fan (Flakt, FAC-6-280-10-12), an auxiliary compressor for pneumatically controllable blade pitch and the tunnel. There are a honeycomb and five screens, and the contraction ratio is nine. The constant-area test section is 1.2 m x 1.8 m and 2.7 m long. The maximum speed is up to 70 m/s, which is evaluated by the differential pressure between the inlet and the exit of contraction section (Chung 1996). As mentioned above, Chung *et al*. (2008) indicated Reynolds number independence for the present test configuration. Thus experiments were conducted at 40 m/s only. It also noted the turbulence intensity of freestream flow was about 0.3%.

For the baseline case, a 60% scaled commercial system (a flat panel of 0.6 m x 1.2 m and a cylinder, 0.27 m in diameter and 0.7 m in length) was fabricated. There is no artificial roughness on the flat panel and cylinder. The lower surface of the flat panel, in which the tilt angles α are 15°, 20°, 25° and 30°, faces the flow direction. This is considered to be the worst case in terms of wind load on a solar collector. Note that the turbulence intensity of incoming flow at low elevation on rooftops might be up to 20-30 percents (Cao *et al*. 2009). A preliminary study by Chou (2009) indicated the uplift force for a solar collector model decreased with increasing turbulence intensity (14%). Since the main objective of the present study is to examine the strong winds on a solar collector, the effect of a steady wind is of first consideration instead of a simulated atmospheric boundary layer. It is also noted that the blockage ratio effect was not corrected. For a real flow simulation with the present test configuration, smaller scaled model tests and full scale model tests in an environmental wind tunnel will be conducted in the future.

For the longitudinal pressure measurements, 26 pressure taps were drilled along the centerline of the upper and lower surfaces of the flat panel. There were no taps on the cylinder. For the lateral pressure measurements (x/c = 0.5), 14 holes were drilled. Tubes were employed to connect the U-tube liquid manometers for evaluating the pressure distributions under different test conditions. Uncertainty of the pressure data was estimated to be 10 Pa. The pressure data were non-dimensionalized by the values of static pressure and dynamic pressure of incoming flow, in which $C_p = (p - p_\infty)/q_\infty$. It is also noted that peak pressure and peak load on the solar collectors are the important information. The dynamic pressure measurements will be conducted in the future study.

For the wind uplift measurements, four load cells (± 1960 N) were installed under the front and rear edges of supporting structure, as shown in Fig. 1b. The load cells were calibrated statically. The uplift coefficient is given as

$$C_{L1} = L/(q_\infty S) \text{ or } C_{L2} = L/(q_\infty S_p)$$

where L is the uplift force, S and S_p are the surface area and projected area of the flat panel. Furthermore, three solid guide plates (0.70 m in width and 0.005 m in thickness) were fabricated for reduction of wind uplift. The height h was 0.35 m (G1), 0.175 m (G2) and 0.1 m (G3), respectively. The guide plate was connected to the junction of the flat panel and the cylinder with two orientation angles (η = 45^o and 90^o) with respect to the wind direction, respectively, as shown in Fig. 1.

3. Results and discussion

3.1 Surface pressure distributions

For a solar collector model with α = 25^o, Chung et al. (2008) indicated that the local loads were significant near the front edge. Reduction in uplift force was observed with a guide plate (G1). For the present study, two more guide plates with different sizes (G2 and G3) were adopted in order to understand further the effects of the guide plate installment on the reduction in uplift force. As shown in Fig. 2 (α = 25^o and V = 40 m/s), the pressure coefficients (G2 plate η = -45^o and 0^o) on the lower surface of the flat panel C_{pl} are roughly the same as those of the baseline case. A slightly higher positive action is observed near the front edge (x/c ≈ 0.3) at η = 45^o, and an uniform negative pressure action is found when the guide plate is normal to the wind direction (η = 90^o). On the upper surface of the flat panel, more flattened pressure coefficients C_{pu} (that is, less suction near the front edge) can be readily observed at η = 90^o. According to the above observations, the guide plate at η = -45^o and 0^o has a minor influence on C_{pl} and C_{pu}, respectively. Thus for the other test cases (α = 15^o, 20^o and 30^o), the guide plates are set up only at 45^o and 90^o

The streamwise distributions of differential pressure coefficient ΔC_p, $(p_l-p_u)/q_\infty$ for the baseline cases (without guide plate) are shown in Fig. 3. Positive pressure action can be seen near the front edge for α = 20^o, 25^o, and 30^o. Then minima are observed in the region of x/c = 0.3-0.4 followed

(a) Baseline model

Fig. 1 Continued

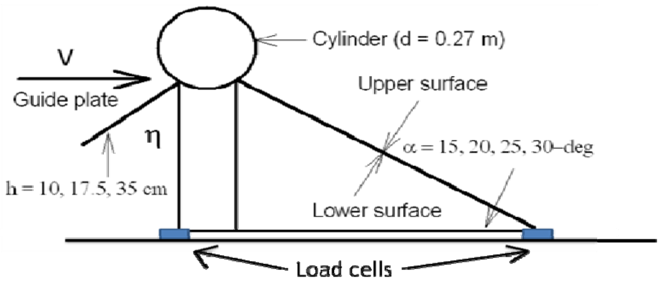

(b) Baseline model with a guide plate

Fig. 1 Test configuration

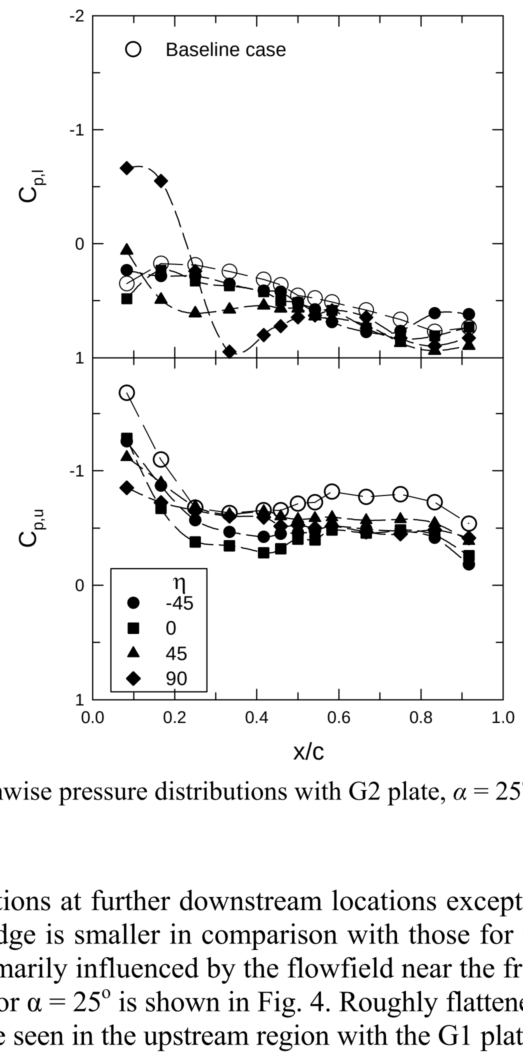

Fig. 2 Streamwise pressure distributions with G2 plate, $\alpha = 25^o$ and V = 40 m/s

by flattened ΔC_p distributions at further downstream locations except to the end of panel. For $\alpha = 15^o$, ΔC_p near the front edge is smaller in comparison with those for the other cases. This implies that the uplift force is primarily influenced by the flowfield near the front edge of the tilt flat panel. With a guide plate, ΔC_p for $\alpha = 25^o$ is shown in Fig. 4. Roughly flattened distributions of differential pressure coefficient can be seen in the upstream region with the G1 plate at $\eta = 90^o$. With G2 and G3 plates (decreasing length), the regions of flattened ΔC_p are reduced. The location of peak ΔC_p moves downstream, where x/c ≈ 0.25, 0.32 and 0.59 for G3, G2 and G1 plates, respectively. This might correspond to the change of the impingement location of the shear layer from the tip of a guide plate on the lower surface of the flat panel. For $\eta = 45^o$, ΔC_p is considerably higher than that for $\eta = 90^o$ for each tested guide plate. For the test cases at $\alpha = 15^o$, 20^o and 30^o, similar trends are also observed. Thus, it is postulated that reduction in local loads near the front edge of a tilt flat panel is attributed to the decrement of the projected area of a guide plate.

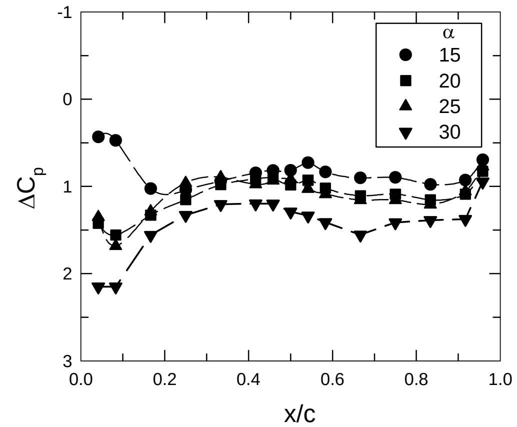

Fig. 3 Streamwise distributions of differential pressure (baseline case)

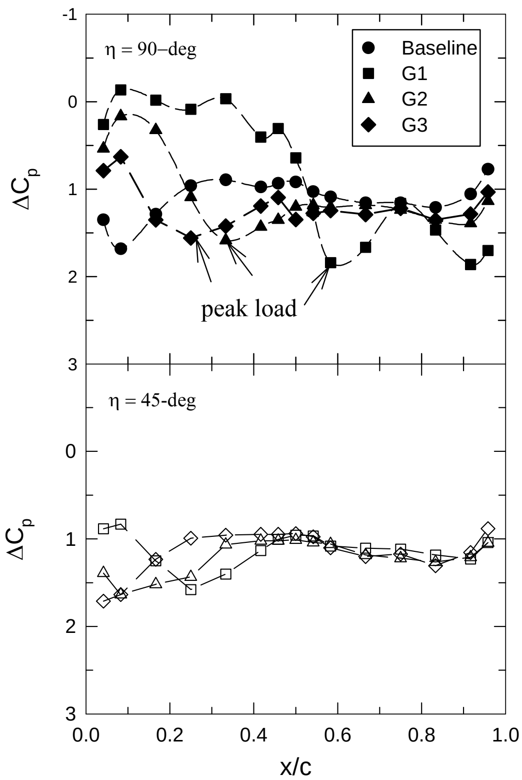

Fig. 4 Streamwise distributions of differential pressure coefficient with guide plates, $\alpha = 25^o$

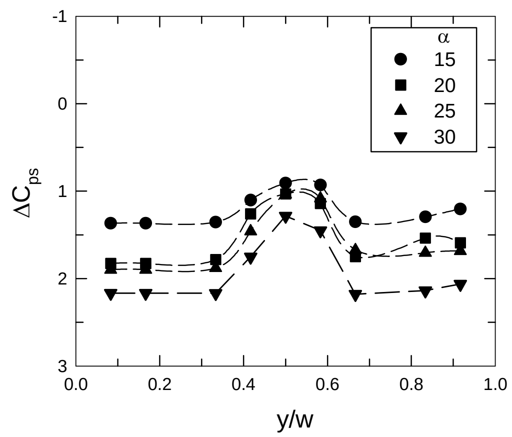

Fig. 5 Spanwise differential pressure distributions (baseline case)

The spanwise (or lateral) pressure distributions are also of interest. These data provide information indicating the three-dimensional effect or corner vortices. In particular, the present experimental program is only for an isolated solar collector model. Investigation on the spanwise pressure distributions would be crucial for the future study of solar collectors in parallel. For the baseline cases, the spanwise differential pressure distributions ΔC_{ps}, $(p_{l,s}-p_{u,s})/q_{\infty}$, are shown in Fig. 5. The inverted U-shaped distributions near the centerline can be seen for all the test cases. This clearly indicates the footprints of corner vortices. With a guide plate, ΔC_{ps} for $\alpha = 25^{o}$ is shown in Fig. 6. As can be seen, the pressure variation in the spanwise direction is diminished with the G1 plate at $\eta = 90^{o}$. For other test cases, decrease in ΔC_{ps} is also observed. This indicates that the guide plates tend to reduce the strength of corner vortices. Furthermore, uniformity of spanwise pressure for a tilt flat panel with a guide plate is also considered to be associated with corner vortices. In Fig. 7, the normalized spanwise differential pressure fluctuation coefficient $C^*_{ps'}$ corresponds to the deviation of $C_{ps'}$ from the baseline cases, which is defined as $(C_{ps',baseline}-C_{ps'})/ C_{ps',baseline}$. The data are plotted versus the projected area ratio of each guide plate on the tilt flat panel.

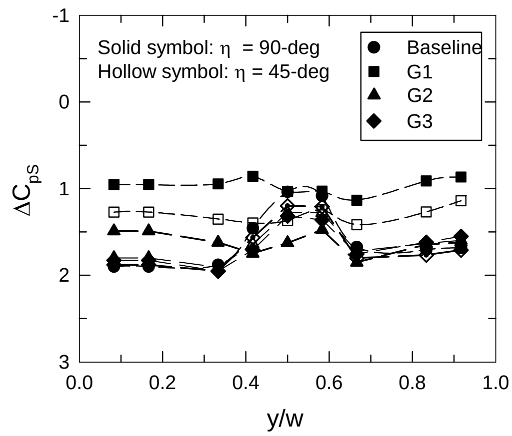

Fig. 6 Spanwise differential pressure distributions, $\alpha = 25^{o}$

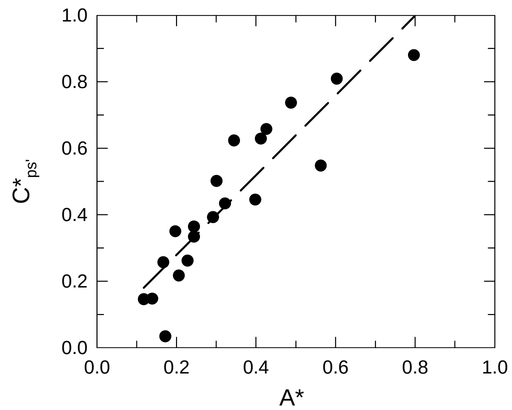

Fig. 7 Dependence of spanwise pressure on A*

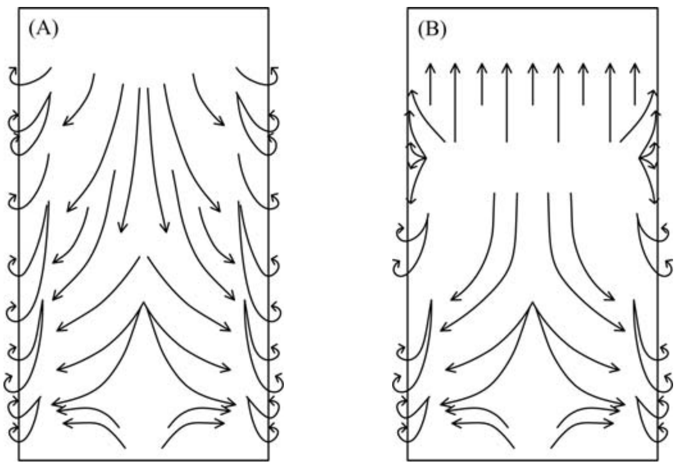

(a) Baseline case and (b) with G1 guide plate at $\eta = 90^o$

Fig. 8 Schematic drawing of oil flow patterns (lower surface)

Although the data are a little scattered, it can be concluded that $C^*_{ps'}$ increases with larger projected area ratio. This is attributed to the attenuation of corner vortices, which also implies the reduction in uplift load of a tilt flat panel with a guide plate. Furthermore, the oil-flow visualization technique is used to visualize the surface flow pattern, which can be used to compare with the surface pressure measurements. A thin film of the mixture (titanium dioxide, oil, oleic acid and kerosene) is applied on the upper and lower surface of the flat panel. A schematic drawing of the flow pattern on the lower surface with and without a guide plate ($\alpha = 25^o$, G1 at $\eta = 90^o$) is shown in Fig. 8. For the baseline case, the corner vortices can be seen clearly. With the guide plate, a cavity is formed between the guide plate and the tilt flat panel. The streamlines within the projected area of the guide plate are nearly straight and parallel to the incoming flow direction. This postulates the attenuation of corner vortices as seen from the mean surface pressure measurements. It also implies that the reduction in the uplift of a tilt flat panel is associated with the projected area of a guide plate.

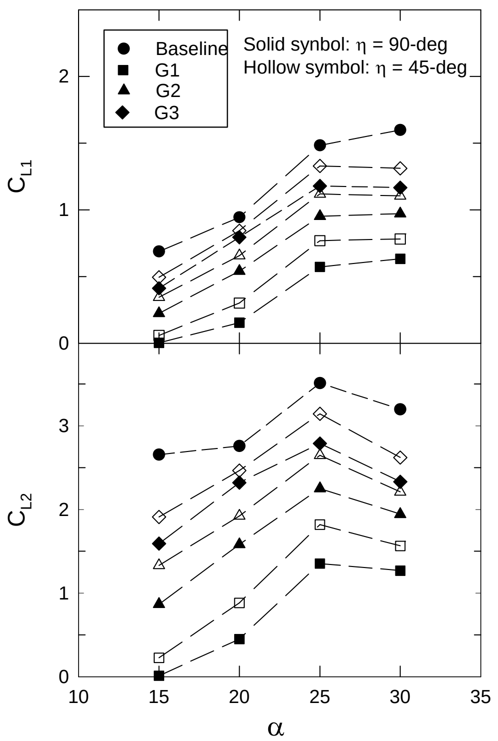

Fig. 9 Dependence of uplift coefficient on the tilt angle

3.2 Wind uplift

For the uplift measurements, the uplift coefficients for all the test cases are shown in Fig. 9. C_{L1} and C_{L2} correspond to the uplift coefficient based on the area and projected area of the flat panel, respectively. For the baseline cases, C_{L1} increases linearly with the tilt angle of the flat panel except for the case of 30^o. With a guide plate, similar phenomena are also observed. For C_{L2}, it appears that a linear relation is no longer valid for the baseline case. Further, reduction in uplift coefficient is observed for the tilt flat panel with a guide plate, particularly with a larger size of guide plate at η= 90^o. The data are re-plotted versus projected area ratio A* in Fig. 10. It is clear that the uplift coefficient (C_{L1} and C_{L2}) for all tilt flat panel decreases linearly with larger projected area of a guide plate. Furthermore, it is known that the lift coefficient of a flat panel could be scaled with the tile angle. Then the slope of uplift coefficient $C_{L\alpha}$, which is equal to 2π based on the thin-airfoil theory, could be adopted to evaluate the characteristic surface area. As shown in Fig. 11, only the test cases of 15^o, 20^o and 25^o were used. It can be seen that $C_{L\alpha,1}$ for all the test cases are roughly the same, but not for $C_{L\alpha,2}$. This indicates that the surface area of the tilt flat panel would be more appropriate as the characteristic area to estimate the uplift coefficient for the present test configurations.

The main theme of the present study is to demonstrate the reduction in uplift of a solar collector model with a guide plate. According to the above observations of spanwise differential pressure distributions and the characteristics of uplift coefficients, it appears that reduction in uplift ΔC_{L1} is

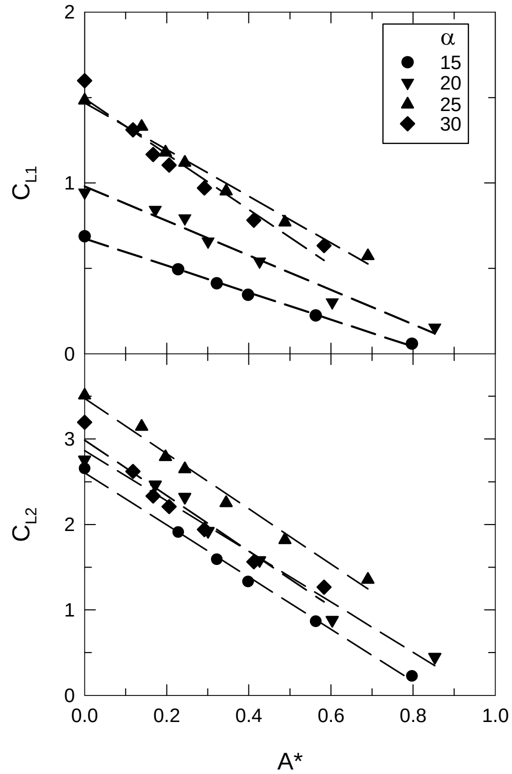

Fig. 10 Reduction in uplift coefficient with respect to A*

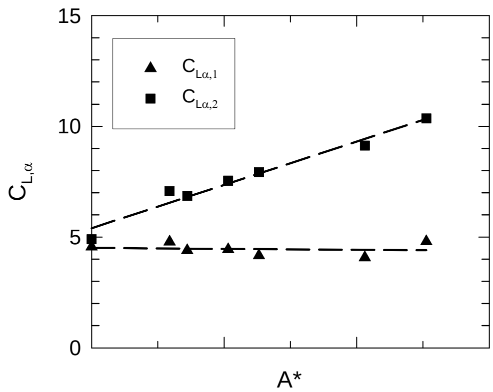

Fig. 11 Slope of uplift coefficient

mainly associated with the projected area ratio of a guide plate on the tilt flat panel. A correlation of uplift reduction and projected area ratio is thus presented in Fig. 12. As can be seen, ΔC_{L1} increases linearly with A*. This indicates that a guide plate with sufficiently large projected area can be employed to reduce the uplift of a tilt flat panel effectively.

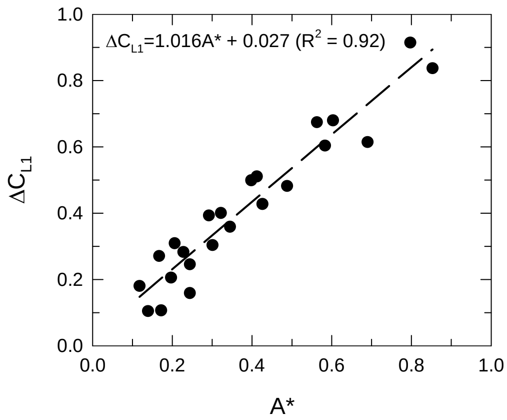

Fig. 12 Reduction in uplift with projected area ratio of guide plate and tilt flat panel

4. Conclusions

Investigation on the mean surface pressure distributions and uplift coefficients of an isolated solar collector model was performed. The present study focuses on the effects of tilt angle of a solar collector and the geometry of a guide plate. It is found that the uplift force is mainly associated with the local load near the front edge and is increased with the tilt angle of the flat panel. Less positive pressure action on the lower surface is observed in the longitudinal direction for the tilt flat panel with installing a guide plate, particularly for the case normal to the wind direction. Uniformity of spanwise differential pressure distribution decreases with larger projected area, and a similar trend is also observed for uplift coefficient. In particular, reduction in wind uplift is correlated reasonably well with the projected area ratio of guide plate and tilt flat panel.

Acknowledgements

This work is under the support by Bureau of Energy, Ministry of Economic Affairs. The assistance by Mr. Y. Wang and Mr. G. Chen at ASTRC/NCKU is also highly appreciated

References

Cao, S., Tamura, Y., Kikuchi, N., Saito, M., Nakayama, I. and Matsuzaki, Y. (2009), "Wind characteristics of a strong typhoon", *J. Wind Eng. Ind. Aerod.*, **97 (1)**, 11-21.

Chang, K.C., Lee, T.S. and Chung, K.M. (2006), "Solar water heaters in Taiwan", *Renew. Energ.*, **31**(9), 1299-1388.

Chang, K.C., Lee, T.S., Lin, W.M. and Chung, K.M. (2008), "Outlook for solar water heaters in Taiwan", *Energ. Policy*, **36**(1), 66-72.

Chang, K.C., Lin, W.M., Lee, T.S. and Chung, K.M. (2009), "Local market of solar water heaters in Taiwan: review and perspectives", *Renew. Energ. Rev.*, **13**, 2605-2612.

Chang, Y.C., Tseng, R.S. and Centurioni, L.R. (2010), "Typhoon-induced strong surface flows in the

Taiwan strait and Pacific", *J. Oceanography*, **66**(2), 175-182.
Chou, J.C. (2009), *Study of aerodynamic effects of solar water heater with a water storage tank*, Master thesis, National Cheng Kung University.
Chung, K.M. (1996), *Calibration of ASTRC/NCKU LWT46 low-speed wind tunnel*, Technical report, Aerospace Science and Technology Research Center, National Cheng Kung University.
Chung, K.M., Chang, K.C. and Liu, Y.M. (2008), "Reduction of wind uplift of a solar collector model", *J. Wind Eng. Ind. Aerod.*, **96**(8-9), 1294-1306.
Holmes, J.D. (2001), *Wind loading of structures*, Spon Press, London, 72-79.
Kalogirou, S. (2004), "Solar thermal collectors and applications", *Prog. in Energy and Combustion Sci.*, **20**, 231-295.
Lee, T.L. (2009), "Predictions of typhoon storm surge in Taiwan using artificial neural networks", *Adv. Eng. Software*, **40** (11), 1200-1206.
Li, Q.S., Xiao, Y.Q., Wu J.R., Fu, J.Y. and Li Z.N. (2008), "Typhoon effects on super-tall buildings", *J. Sound Vib.*, **313**(3-5), 581-602.
Li, H.W., Tsai, C.H. and Lo, Y.T. (2009), "Numerical simulation of typhoon surges along the coast of Taiwan", *Nat. Hazards*, **50**(3), 413-431.
Oaulotto, C., Ciampoli, M. and Augusti, G. (2006), "Wind tunnel evaluation of mean wind pressure on a frame-type signboard", *J. Wind Eng. Ind. Aerod*., **94**(5), 397-413.
Radu, A., Axinte, E. and Theohari, C. (1989), "Steady wind pressures on solar collectors on flat-roofed buildings", *J. Wind Eng. Ind. Aerod.*, **23**, 249-258.
Wood, G.S., Denoon, R. and Kwok, K. (2001), "Wind loads on industrial solar panel arrays and supporting roof structure", *Wind Struct*., **4**(6), 481-494.

Nomenclature

A_p	projected area of guide plate
A*	projected area ratio, A_p/S_p
c	length of flat panel
C_p	pressure coefficient, $(p - p_\infty)/ q_\infty$
C_{L1}	uplift coefficient, $L/(q_\infty S)$
C_{L2}	uplift coefficient, $L/(q_\infty S_p)$
$C_{L\alpha}$	derivative of uplift coefficient with α
h	height of guiding plate
L	uplift force, N
p_l	lower surface pressure at longitudinal direction
p_u	upper surface pressure at longitudinal direction
$p_{l,s}$	lower surface pressure at spanwise direction
$p_{u,s}$	upper surface pressure at spanwise direction
q_∞	dynamic pressure
S	surface area of flat panel
S_p	projected area (to the incoming flow)of flat panel
V	speed of incoming flow, m/s
w	width of flat panel
x	distance along the centerline of flat panel, x = 0 indicating top position
y	lateral distance, y = 0 indicating left end
ΔC_p	streamwise differential pressure coefficient, $(p_l-p_u)/ q_{\infty\infty}$
ΔC_{ps}	spanwise differential pressure coefficient, $(p_{l,s}-p_{u,s})/q_\infty$
ΔC_{L1}	reduction of uplift coefficient $(C_{L1,baseline}-C_{L1})/C_{L1,baseline}$
α	tilt angle of flat panel, deg
η	orientation of guide plate, deg